Voigt-function model in diffraction line-broadening analysis

Davor Balzar

Materials Science and Engineering Laboratory

National Institute of Standards and Technology

Boulder, Colorado 80303

and

Physics Department

University of Colorado

Boulder, CO 80309

Abstract

Diffraction-line broadening routes are briefly reviewed. Both laboratory and synchrotron x-ray measurements of W and MgO showed that a Voigt function satisfactorily fits the physically broadened line profiles. The consequences of an assumed Voigt-function profile shape for both size-broadened and strain-broadened profiles ("double-Voigt" method) are studied. It is shown that the relationship between parameters obtained by the Warren-Averbach approximation and integral-breadth methods becomes possible. Line-broadening analysis of W and MgO is performed by using the Warren-Averbach and "double-Voigt" approaches and results are compared.

List of symbols

a, b, c,	
m, m′,	
U, V, W	General constants
z	General variable
A	Fourier coefficient
a_3	Edge of orthorhombic cell, orthogonal to diffracting planes
D	"Apparent" domain size orthogonal to diffracting planes
d	Interplanar spacing
e	"Maximum" (upper limit) strain
FWHM	Full width at half maximum of profile
f, F	Pure-specimen (physically) broadened profile and its Fourier transform
g, G	Instrumentally broadened profile and its Fourier transform
h, H	Observed broadened profile and its Fourier transform
hkl	Miller indices
I	Intensity
K	Scherrer constant
k	$\beta_C/(\pi^{1/2}\beta_G)$, characteristic integral-breadth ratio of a Voigt function
L, L'	na_3, column length (distance between two cells in a real space) orthogonal to diffracting planes
l	Order of reflection
MSS	Mean-square strain
n	Harmonic number

p	Column-length distribution function
R	Relative error
RMSS	Root-mean-square strain
s	$2\sin\theta/\lambda = 1/d$, variable in reciprocal space
x	Data-sampling variable: either 2θ or s
β	$\beta(2\theta)\cos\theta_0/\lambda$, integral breadth in units of s (Å^{-1})
γ	Geometrical-aberration profile
$<\epsilon^2(L)>$	Mean-square strain, orthogonal to diffracting planes, averaged over the distance L
η	"Apparent" strain
θ	Diffraction angle
θ_0	Bragg angle of $K\alpha_1$ reflection maximum
λ	X-ray wavelength
ω	Wavelength-distribution profile

SUBSCRIPTS

C	Denotes Cauchy (Lorentz) function
D	Denotes distortion-related parameter
f	Denotes physically (pure-specimen) broadened profile
G	Denotes Gauss function
g	Denotes instrumentally broadened profile
h	Denotes observed broadened profile
m	Denotes a maximum index
S	Denotes size-related parameter
s	Denotes surface-weighted parameter

V	Denotes Voigt function
v	Denotes volume-weighted parameter
wp	Denotes weighted-residual error

OPERATORS

★	Convolution: $g(x) \star f(x) = \int g(z)f(x-z)\mathrm{d}z$

1 Introduction

Phenomenological line-broadening theory of plastically deformed metals and alloys was developed almost 50 years ago (Warren and Averbach 1950; Warren 1959). It identifies two main types of broadening: the size and strain components. The former depends on the size of coherent domains (or incoherently diffracting domains in a sense that they diffract incoherently to one another), which is not limited to the grains but may include effects of stacking and twin faults and subgrain structures (small-angle boundaries, for instance); and the latter is caused by any lattice imperfection (dislocations and different point defects). The theory is general and was successfully applied to other materials, including oxides and polymers. However, the parameters obtained need a careful assessment of their physical validity and correlation to the particular structural features of the material under study. In different approaches (Krivoglaz and Ryaboshapka 1963; Wilkens 1984; Groma *et al.* 1988), the effects of simplified dislocation configurations on diffraction-line broadening were modeled. These theories were applied mainly to the plastically deformed copper single crystals and recently to the γ'-precipitate-hardened nickel-base superalloy (Kuhn *et al.* 1991). These microscopic models correctly identify origins of broadening in the terms of physically recognized quantities. As our understanding and ability to model complex systems develops further, it is expected that their application will gradually include other materials where different sources of line broadening usually occur simultaneously. The focus here is to study and compare methods of line-broadening analysis in the frame of phenomenological approaches.

The development of this research field began when Scherrer (1918) understood that small crystallites cause broadening of diffraction lines. However, more than quarter of a century elapsed before a more complex and exact theory of line broadening was formulated by Stokes and Wilson (1944). They included the lattice strain as another source of broadening. Shortly thereafter, a new impulse was given to the theory: Stokes (1948) adapted the Fourier-deconvolution method to obtain the purely physical broadened line profiles from the observed pattern. Instead of mere estimates of

either average size of coherent domains or some measure of strain, through the developments of Bertaut (1949) and Warren and Averbach (1950; 1952), a more detailed analysis of complete line-profile shape became possible. Moreover, Wilson (1962a) introduced the analysis of the variance of profile, and Ergun (1968) the method of successive foldings. All those procedures pushed aside the integral-breadth methods because of the important advantage of model independence. Moreover, with a careful application, it was possible to obtain much more information, such as column-length distribution function, the behavior of strain as a function of the averaging distance in domains, *etc*. However, they also have very serious drawbacks: in cases of large line overlapping, or weak structural broadening, the Stokes deconvolution method cannot be applied without severe errors. This limits application to a small number of specimens and to cubic crystal systems. Moreover, the mathematical process involved is cumbersome and difficult to apply straightforwardly. This is why, after the development of the Rietveld (1967) refinement and other full-powder-pattern-fitting techniques (Pawley 1981; Toraya 1986), the integral-breadth fitting methods became attractive again. After Langford (1978) introduced a Voigt function in the field of x-ray powder diffraction, it was quickly adopted in the Rietveld analysis (Ahtee *et al.* 1984), along with its approximations (Young and Wiles 1982). It proved to be satisfactory and flexible enough for most purposes when angle dependence of parameters is modeled properly.

Alternatively, although the Stokes method has put severe limitations on the analysis, the Warren-Averbach method of separation of size-strain broadening has remained the least constrained method for analyzing diffraction-line broadening. The parameters obtained through the Warren-Averbach and integral-breadth methods are differently defined, and thus not necessarily comparable. The main intention here is to study these two different courses of line-broadening analysis and show their equivalence under the following circumstances: both size-broadened and strain-broadened line-profiles are modeled with a Voigt function and distance-averaged strain follows the Gauss distribution (Balzar and Ledbetter 1993). The first condition also defines the total physically broadened profile

6

as a Voigt function. Laboratory and synchrotron x-ray diffraction experiments were performed on W and MgO powders to study the feasibility of the simple Voigt-function modeling in line-broadening analysis. The physically broadened line profiles obtained through two different approaches, namely Stokes deconvolution and convoluted-profile fitting, are compared. Furthermore, the Warren-Averbach and integral-breadth methods are applied to the so-obtained respective physically broadened line profiles, and differences are assessed.

2 Diffraction-line broadening

Both instrument and specimen broaden the diffraction lines, and the observed line profile is a convolution (Taupin 1973):

$$h(x) = g(x) \star f(x) + \text{background.} \tag{1}$$

Wavelength distribution and geometrical aberrations are usually treated as characteristic of the particular instrument (instrumental profile):

$$g(x) = \omega(x) \star \gamma(x). \tag{2}$$

To obtain microstructural parameters of the specimen, the physically (specimen) broadened profile f must be extracted from the observed profile h.

Origins of specimen broadening are numerous. Generally, any lattice imperfection will cause additional diffraction-line broadening. Therefore, dislocations, vacancies, interstitials, substitutional, and similar defects lead to lattice strain. If a crystal is broken into smaller incoherently diffracting domains by dislocation arrays (small-angle boundaries), stacking faults, twins, large-angle boundaries (grains), or any other extended imperfections, then domain-size broadening occurs.

2.1 Instrumental broadening

The first step before any attempt to analyze diffraction-line broadening is to correct the observed line profiles for instrumental effects. A careful scan of a suitable standard sample, showing minimal physical broadening will define the instrumental contribution to broadening. Thorough recipes for preparing the standard specimen are given elsewhere (Berkum *et al.* 1995).

Previously, to obtain a standard, it was customary to anneal the specimen showing broadened reflections. This was the most desirable approach when the Stokes deconvolution method was applied because the centroids of *f* and *g* should be as close as possible. However, very often a material does not give satisfactorily narrow lines. It is becoming more customary to find a suitable certified standard reference material which allows a true comparison of results among different laboratories. Because the lines of standard and studied specimen usually do not coincide, it is required to model the characteristic parameters of the standard's line-profile shapes analytically so that the needed instrumental profile can be synthesized at any angle of interest. Most often, the original Caglioti *et al.* (1958) relation is used:

$$\text{FWHM}^2(2\theta) \;=\; U\tan^2\theta + V\tan\theta + W. \tag{3}$$

This function was derived for neutron diffraction. Although not theoretically justified, it was confirmed to satisfactorily model as well the angular variation of the symmetrical part of x-ray diffraction-line-profile width. Contrary to the requirement on the physically broadened line profile, it is most important for the instrumental function to correctly describe the angular variation of parameters, regardless of its theoretical foundation. The asymmetry is most often modeled by the split-Pearson VII function (Hall *et al.* 1977), where the angular variation of the Pearson-VII "shape" parameter *m* can be simply defined as (Howard and Snyder 1989):

$$m(2\theta) \;=\; a\,(2\theta)^2 \;+\; b\,(2\theta) \;+\; c. \tag{4}$$

Therefore, for a description of asymmetric instrumental broadening, three parameters from both (3)

and (4) for each low-angle and high-angle side of the profiles are needed.

2.2 Extraction of physically broadened line profile

The choice of the method to obtain the parameters of pure physically broadened line profiles is of utmost importance for the subsequent line-broadening analysis. Basically, the methods used can be divided in two groups: (i) deconvolution approach where the physically broadened line profile is unfolded from the observed profile using the previously determined instrumental profile; (ii) convolution approach where, contrary to the former, the observed profile is built according to (1) and adjusted to the observed pattern through a least-squares fitting. However, we have a knowledge of h and g, but not of f. Therefore, both the general type and parameters of f are assumed, which introduces a bias in the method. Nevertheless, with the development of Rietveld and similar algorithms, where all the parameters are determined in this way anyhow, this approach can be built into the code in parallel to the structural and other parameters and refined simultaneously, whereas deconvolution procedures are much more complicated to introduce. Another important difference between the two approaches is that deconvolution methods under some circumstances either fail or become unstable and inaccurate. The convolution process is always stable, but, beside the systematic errors introduced by a possible inadequate model of physically broadened line profile, the iterative least-squares minimization procedure can be trapped in a false minimum. Moreover, the smallest reliability index does not necessarily correspond to a physically meaningful solution; for instance, adding more peaks in refinement than actually exist may decrease it. For some illustrations and possible artifacts of profile fitting, see Howard and Preston (1989), and for an example of how a high degree of line overlap may influence size-strain analysis see Balzar (1992).

The most used of the first type is the Fourier-transform deconvolution method (Stokes 1948), although there are some novel approaches (Kalceff *et al.* 1995) using constrained Phillips-Twomey (Twomey 1963) or maximum-entropy deconvolution (Skilling and Bryan 1984) methods. Another

(in fact deconvolution) process, although accomplished by simple substraction of the instrumental-profile variance (Wilson 1962a) is not used extensively, and will not be considered here. Likewise, among the methods falling into the second group, the iterative method of successive foldings (Ergun 1968) is used sparingly, and will not be considered. Some new developments can be found in the review by Reynolds (1989).

2.2.1 <u>Deconvolution method of Stokes</u>

From (1), it follows that deconvolution can be performed easily in terms of complex Fourier transforms of respective functions:

$$F(n) = \frac{H(n)}{G(n)}.$$ (5)

The inverse Fourier transform gives a physically broadened line profile:

$$f(x) = \sum_n \frac{H(n)}{G(n)} \exp\left(-\frac{2\pi i x n}{x_m}\right).$$ (6)

Hence, the physically broadened profile f is retrieved from the observed profile h without any assumption (bias) on the peak-profile shape. However, (5) may not give a solution if the Fourier coefficients of the f profile do not vanish before those of the g profile (Delhez *et al.* 1980). Furthermore, if physical broadening is small compared with instrumental broadening, deconvolution becomes too unstable and inaccurate. If the h profile is 20% broader than the g profile, this gives an upper limit of about 1000 Å for the determination of the effective domain size (Schwartz and Cohen 1977). Regardless of the degree of broadening, deconvolution produces unavoidable profile-tail ripples because of truncation effects. To obtain reliable results, errors of incorrect background, sampling, and the standard specimen have to be corrected (Delhez *et al.* 1986; 1988). The largest conceptual problem, however, is peak overlapping. If the complete peak is not separated, the only possible solution is to try to reconstruct the missing parts. This requires some assumption on the

peak-profile shape, which introduces bias into the method. The application of the strict Stokes method is therefore limited to materials having the highest crystallographic symmetry.

2.2.2 Convolution-fitting methods

Here it is required that at least the unknown physically broadened diffraction profile f be approximated with some analytical function. In the past, two commonly used functions were Gauss

$$I(x) \ = \ I(0) \ \exp \left(-\pi \frac{x^2}{\beta_G^2} \right) \tag{7}$$

and Cauchy (Lorentz)

$$I(x) \ = \ I(0) \ \frac{1}{\dfrac{\beta_C^2}{\pi^2} \ + \ x^2}. \tag{8}$$

From the convolution integral (1), it follows that for Cauchy profiles

$$\beta_{hC} \ = \ \beta_{gC} \ + \ \beta_{fC} \tag{9}$$

and for Gauss profiles

$$\beta_{hG}^2 \ = \ \beta_{gG}^2 \ + \ \beta_{fG}^2. \tag{10}$$

However, the observed x-ray diffraction line profiles cannot be well represented with a simple Cauchy or Gauss function (Klug and Alexander 1974; Young and Wiles 1982). Experience shows that the Voigt function, or its approximations, pseudo-Voigt (Wertheim *et al.* 1974) and Pearson-VII (Hall *et al.* 1977) fit very well the observed peak profiles in both x-ray and neutron-diffraction cases. The Voigt function is usually represented following Langford (1978):

$$I(x) \ = \ I(0) \left(\frac{\beta}{\beta_C} \right) \ \mathrm{Re} \left[\mathrm{erfi} \left(\frac{\pi^{1/2}x}{\beta_G} \ + \ ik \right) \right]. \tag{11}$$

Here, the complex error function is defined as

$$\mathrm{erfi}(z) = \exp(-z^2)\ \mathrm{erfc}(-iz) \qquad (12)$$

and erfc denotes the complementary error function.

Integral breadth of the Voigt function is expressed through its constituent integral breadths (Schoening 1965):

$$\beta = \beta_G \frac{\exp(-k^2)}{\mathrm{erfc}(k)}. \qquad (13)$$

Halder and Wagner (1966) showed that the following parabolic expression is a satisfactory approximation:

$$\beta^2 = \beta_C\,\beta + \beta_G^2. \qquad (14)$$

Because convolution of two Voigt functions is also a Voigt function, integral breadths are easily separable conforming to (9) and (10).

In case that any of h, g, or f profiles are asymmetric, they cannot be modeled with the discussed functions. Indeed, for Bragg-Brentano geometry, observed diffraction-line profiles are asymmetric toward the low-angle side for small diffraction angles and switch to a slight reverse asymmetry at the highest diffraction angles. Asymmetry is introduced in g by axial beam divergency, specimen transparency and flat surface (Klug and Alexander 1974). However, extrinsic stacking and twin faults may introduce (relatively weak) asymmetry in f also (Warren 1969). Unfortunately, numerical convolutions are usually necessary in these cases, thus consuming calculation time and introducing additional errors. This is why asymmetry is often neglected. However, it may cause large errors in line-broadening analysis. Some examples of numerical convolutions used are the following: Enzo *et al.* (1988) modeled g with a pseudo-Voigt convoluted with the exponential function and f with a pseudo-Voigt; Howard and Snyder (1989) modeled g with a split-Pearson VII and f with a Cauchy function, whereas Balzar (1992) modeled g also with a split-Pearson VII but f with a Voigt function. There were no attempts yet to assume an asymmetrical f profile.

12

2.2.3 Physically broadened profiles of W and MgO

The Stokes Fourier-deconvolution method followed by the Warren-Averbach analysis of physically broadened line profile is the least biased approach to the analysis of line broadening. The opposite procedure is profile fitting of the convolution of the presumed analytical function, which models the physically broadened line profile and instrumental profile obtained by measuring a suitable standard material and consecutive application of some integral-breadth method. Both approaches have advantages and disadvantages and it is generally assumed that different results are obtained. The critical step is a correction for instrumental broadening. Because of numerous problems associated with the Fourier deconvolution and especially the inevitable ripples at tails of physically broadened profile, there were almost no attempts to fit it with some analytical function. Suortti *et al.* (1979) fitted a Voigt function to the least-squares deconvoluted profiles of a Ni powder and found good overall agreement. Reynolds (1989) fitted successfully a pseudo-Voigt function to the physically broadened line profiles of chlorite, obtained by the Ergun (1968) method of iterative folding. Although different approaches to deconvolution are possible, we used the Stokes method because of its wide acceptance. Many different integral-breadth routes were used in the literature. We followed our previous studies (Balzar 1992).

2.2.3.1 Materials

Two "classical" materials for line-broadening analysis, W and MgO, were selected because of their simple cubic structure (the Stokes method is optimally applicable) and different origins of broadening; It is expected that on cold deformation, W shows dominantly strain broadening caused by introduction of numerous dislocations, whereas the thermal decomposition of $MgCO_3$ gives rise to size broadening only. W is elastically isotropic and shows well-resolved reflections thus admitting a relatively large number of reflections to be analyzed simultaneously. Likewise, because of negligible strain and low probability of fault formation in MgO, a simultaneous treatment of all

accessible reflections is possible. W powder of nominal size 8-12 µm was ball-milled for different times. After some initial milling time no additional change of peak widths was observed. The fine $MgCO_3$ powder was decomposed at different temperatures, $350\,°C$ and higher. The powder was kept at a particular temperature for 3 h and allowed to cool slowly in the furnace to minimize possible lattice defects. As a standard specimen for W, the original untreated W powder was used. It shows minimal line broadening, comparable to the NIST standard reference material LaB_6. The MgO standard was prepared by decomposing the $MgCO_3$ powder at $1300\,°C$ for 6 hours. Although it showed relatively broad reflections (FWHM at $37°$ 2θ was about $0.15°$ 2θ compared to only $0.08°$ 2θ for LaB_6), we used it to get optimal conditions for the Stokes analysis, because the appreciable difference between standard and specimen peak positions represents a problem, and the needed interpolation of Fourier coefficients of the standard would introduce additional uncertainties. Moreover, we were not interested in the absolute magnitude of results. We chose specimens from each batch (W specimen ball milled for 140 min and MgO specimen decomposed at $550\,°C$) showing approximately 3-4 times broader reflections than the respective standards because the Stokes method has optimum application for this factor in the range 2-6 (Delhez *et al.* 1980).

2.2.3.2 *Data analysis*

We collected data with both laboratory and synchrotron x-ray sources. Synchrotron-radiation measurements were performed on the X3B1 powder-diffraction beamline at the National Synchrotron Light Source (NSLS), Brookhaven National Laboratory (BNL). A Si channel-111-cut monochromator, flat specimen, Ge 111-cut analyzer crystal, and proportional detector were used. More details on experimental setup and line-profile shape were published elsewhere (Balzar *et al.* 1997a). Laboratory x-ray data were collected using a horizontal goniometer and counted with a solid-state detector. We used a fixed-time counting method with a condition to collect about 10,000 counts at each peak maximum. The raw data were used in the analysis to avoid introducing any bias by

smoothing methods. However, the deconvolution process is very sensitive to noise in the data and it caused unwanted spurious oscillations in Fourier coefficients, especially for the laboratory x-ray measurements. We measured seven W reflections using Cu $K\alpha$ radiation. The 400 peak was excluded because the high-angle background was not accessible with our goniometer. For the MgO pattern, we analyzed only 220, 400, and 422 reflections because others come in close pairs for the *fcc* structure. The inevitable line overlapping would require the unsafe estimation of missing tails and introduce unwanted bias in the Fourier deconvolution. Linear background was determined by fitting the first-order polynomial to data before applying either Stokes deconvolution or profile fitting. The $K\alpha_2$ elimination prior to the Stokes deconvolution was not performed because it may introduce additional errors. In the convolution-fitting approach, the $K\alpha_2$ component is treated analogously to $K\alpha_1$, but with half its intensity and the same profile shape. After correction for the Lorentz-polarization factor, Stokes deconvolution was performed on a 2θ scale to be in accord with the profile fitting. Hence, for both deconvolution and fitting/convolution approaches, there is a systematic error because the subsequent analyses are implemented in Fourier space. Although it is possible to perform both Stokes deconvolution and profile fitting on the *s* scale, we found the error to be negligible at this or a smaller level of broadening. The origin was taken at the centroid of the standard peak, although there were no substantial shifts of broadened peaks. The convolution-fitting process was performed in the following way: the instrumental profile was obtained by fitting the split-Pearson VII function to the particular line profile of the standard specimen. By convoluting it with the preset physically broadened Voigt function, the "observed" profile is obtained. After adding the previously refined linear background, the parameters of physically broadened Voigt function are adjusted in the least-squares fitting to the observed pattern.

2.2.3.3 Fitting of physically broadened line profiles

Following (6), the physically broadened line profile can be back-synthesized from the Fourier

coefficients obtained by deconvolution. However, because of noise in the raw data, after some harmonic number, Fourier coefficients become unreliable and cause large oscillations in the synthesized profiles (Delhez *et al.* 1980). Typical plots of synthesized physically broadened line profiles are shown in Figures 1 (110 W at low angle) and 2 (422 MgO at high angle). Conversely, the 110 W physically broadened line profile obtained from the synchrotron data (Figure 3) does not show peak-tail ripples. This is unlikely to be caused by statistical noise only; Figure 4 shows the deconvoluted physically broadened line profile of the weakest 400 MgO line where only 900 counts were collected at the peak maximum. It indicates that generally superior synchrotron resolution and simpler (singlet) wavelength distribution allows for more precise line-broadening studies. To test whether simple analytical functions can successfully approximate a physically broadened profile, least-squares fits of Cauchy, Gauss, and Voigt functions to the profiles in Figures 3 and 4 were performed. It is obvious that the Voigt function shows a superior and overall satisfactory fit. Even more important is how different functions fit profiles. Although the Cauchy function approximates tails quite well, it fails to fit profile shapes close to
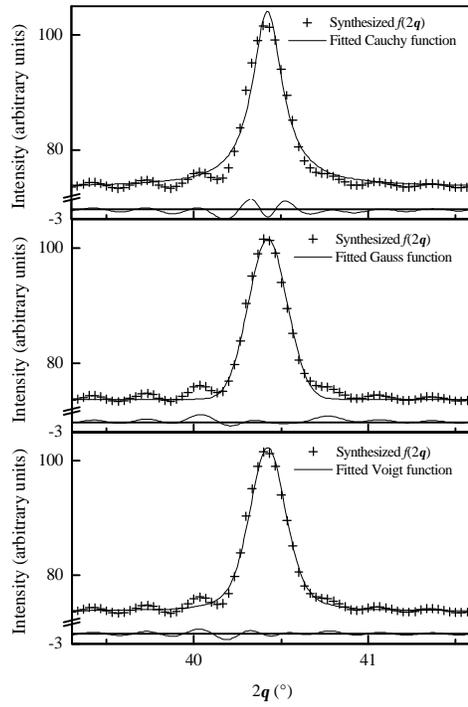
Fig. 1. Cauchy, Gauss, and Voigt-function fits to the Stokes-deconvoluted physically broadened 110 W line profile (laboratory x-ray data). Difference patterns plotted around zero intensity on the smaller scale.
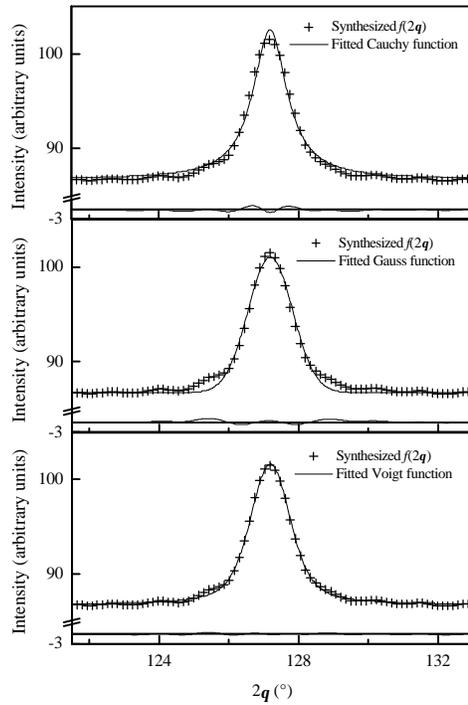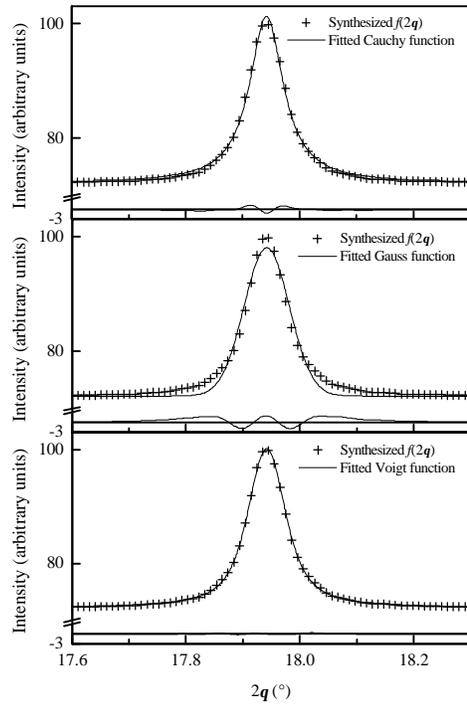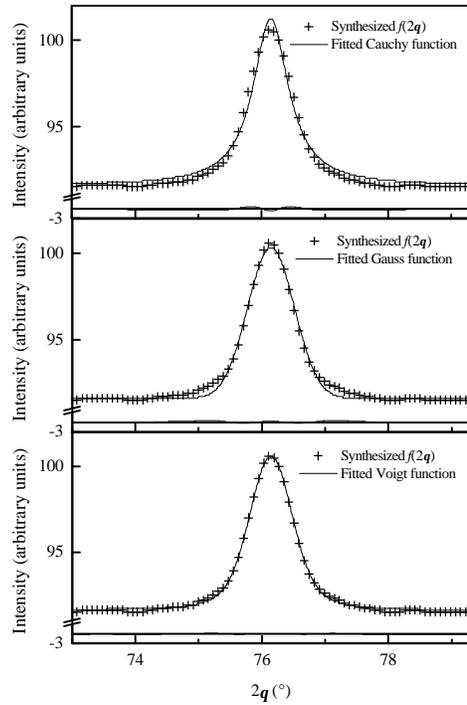

Fig. 2. Cauchy, Gauss, and Voigt-function fits to the Stokes-deconvoluted physically broadened 422 MgO line profile (laboratory x-ray data). Difference patterns plotted around zero intensity on the smaller scale.

Fig. 3. Cauchy, Gauss, and Voigt-function fits to the Stokes-deconvoluted physically broadened 110 W line profile (synchrotron x-ray data). Difference patterns plotted around zero intensity on the smaller scale.

Fig. 4. Cauchy, Gauss, and Voigt-function fits to the Stokes-deconvoluted physically broadened 400 MgO line profile (synchrotron x-ray data). Difference patterns plotted around zero intensity on the smaller scale.

18

Table 1. Least-squares fits to the synthesized physically broadened line profiles of W obtained by the Fourier-deconvolution Stokes (1948) method (laboratory x-ray data).

hkl	Voigt function					Cauchy function		Gauss function	
	β_C	β_G	β	FWHM	R_{wp}	FWHM	R_{wp}	FWHM	R_{wp}
		(° 2θ)			(%)	(° 2θ)	(%)	(° 2θ)	(%)
110	0.141(5)	0.207(3)	0.306	0.250	0.37	0.208(2)	0.64	0.260(1)	0.49
200	0.237(5)	0.221(3)	0.394	0.302	0.29	0.259(2)	0.47	0.328(2)	0.49
211	0.416(6)	0.222(5)	0.544	0.384	0.30	0.347(2)	0.35	0.452(2)	0.52
220	0.460(8)	0.301(6)	0.649	0.472	0.30	0.415(2)	0.37	0.544(3)	0.49
310	0.664(17)	0.190(21)	0.732	0.485	0.55	0.469(5)	0.55	0.620(6)	0.73
222	0.647(17)	0.610(12)	1.083	0.831	0.32	0.690(4)	0.39	0.925(4)	0.41
321	1.243(15)	0.460(15)	1.452	0.984	0.21	0.921(4)	0.23	1.224(7)	0.42

Table 2. Least-squares fits to the synthesized physically broadened line profiles of MgO obtained by the Fourier-deconvolution Stokes (1948) method (laboratory x-ray data).

hkl	Voigt function					Cauchy function		Gauss function	
	β_C	β_G	β	FWHM	R_{wp}	FWHM	R_{wp}	FWHM	R_{wp}
		(° 2θ)			(%)	(° 2θ)	(%)	(° 2θ)	(%)
220	0.427(9)	0.576(6)	0.877	0.708	0.18	0.595(4)	0.39	0.742(3)	0.30
400	0.805(22)	0.593(16)	1.196	0.885	0.33	0.780(6)	0.40	0.984(7)	0.47
422	1.056(13)	1.024(9)	1.794	1.383	0.15	1.184(6)	0.32	1.502(6)	0.32

Table 3. Comparison of Voigt-function fits to the synthesized physically broadened line profiles of W obtained by the Stokes deconvolution method (S.D.) (Table 1) and an assumed physically broadened Voigt profile used in convolution-fitting (C.F.) approach. The agreement index is defined as $R = 100 - 100 \beta$ (C.F.)/β (S.D.).

hkl	β_C (S.D.)	β_C (C.F.)	β_G (S.D.)	β_G (C.F.)	β (S.D.)	β (C.F.)	R
			($^{\circ}$ 2θ)				(%)
110	0.141(5)	0.222(4)	0.207(3)	0.114(7)	0.306	0.286	6.5
200	0.237(5)	0.276(4)	0.221(3)	0.166(6)	0.394	0.377	4.3
211	0.416(6)	0.408(6)	0.222(5)	0.220(9)	0.544	0.535	1.7
220	0.460(8)	0.443(11)	0.301(6)	0.319(13)	0.649	0.651	-0.3
310	0.664(17)	0.567(11)	0.190(21)	0.318(16)	0.732	0.754	-3.0
222	0.647(17)	0.629(33)	0.610(12)	0.633(31)	1.083	1.089	-0.6
321	1.243(15)	0.982(25)	0.460(15)	0.746(29)	1.452	1.479	-1.9

Table 4. Comparison of Voigt-function fits to the synthesized physically broadened line profiles of MgO obtained by the Stokes deconvolution method (S.D.) (Table 2) and an assumed physically broadened Voigt profile used in convolution-fitting (C.F.) approach. The agreement index is defined as $R = 100 - 100 \beta$ (C.F.)/β (S.D.).

hkl	β_C (S.D.)	β_C (C.F.)	β_G (S.D.)	β_G (C.F.)	β (S.D.)	β (C.F.)	R
			($^{\circ}$ 2θ)				(%)
220	0.427(9)	0.638(13)	0.576(6)	0.381(17)	0.877	0.869	0.9
400	0.805(22)	0.803(28)	0.593(16)	0.563(28)	1.196	1.167	2.4
422	1.056(13)	1.140(42)	1.024(9)	0.999(42)	1.794	1.838	-2.5

its maximum. On the contrary, the Gauss function fits fairly well around the peak maximum, whereas tails fall off too rapidly. This is known to be true also for the observed diffraction profiles. Also despite substantial profile-tail ripples, the fits of physically broadened profiles obtained from the laboratory data (Figures 1 and 2) show the same behavior. The complete laboratory x-ray results for both materials are presented in Tables 1 and 2. Line-broadening analysis of synchrotron data will be published elsewhere (Balzar *et al.* 1997b).

Tables 1 and 2 show that the lowest residual indexes are obtained for a Voigt-function fit, despite fewer free parameters. In Tables 3 and 4, we compare the parameters of so-obtained Voigt-function fits to the Voigt function used to model physically broadened line profiles through the convolution fitting. Except for two low-angle W lines, both Cauchy and Gauss integral breadths, and particularly the total integral breadth, agree very well. This discrepancy at low angles is not understood at present, because the instrumental-profile asymmetry was modeled in a convolution-fitting approach. Moreover, the effect or asymmetry is much more pronounced for the synchrotron source at lower angles because of large axial-divergence effect; the synchrotron 110 W deconvoluted profile (Figure 3) is perfectly symmetrical while its laboratory counterpart (Figure 1) shows asymmetry. Therefore, this effect may be caused by the Cu $K\alpha$ doublet.

One may conclude that it seems reasonable to approximate the physically broadened line profile with a Voigt function. Because a convolution of two Voigt function is also a Voigt function, in the subsequent paragraphs we shall emphasize the use of a Voigt function both as a size-broadened and a strain-broadened profile in line-broadening analysis.

3 Size-strain analysis

After removing the instrumental broadening from the observed line profile, it is possible to analyze the physically broadened line profile, to consider the origins and amount of broadening. It was discussed (Delhez *et al.* 1988) that "size" and "strain" terms can be applied only tentatively The size broadening describes all the possible effects that could be put in the common category "coherent domain size", that is, the size of domains distinctly defined by coherent diffraction, such as stacking (deformation) or twin (growth) faults, small-angle boundaries caused by dislocation ordering, grains, or similar extended lattice defects. This is why x-ray domain size sparingly amounts to the particle or grain size, measurable by other, mostly optical, methods (microscope, laser-size analyzer, etc.). Alternatively, the strain term includes contributions from any disruption of a regular lattice, such as dislocations and different point defects. It follows that these two effects are interconnected; dislocations cause strain but also arrange into boundaries between incoherently diffracting domains.

21

This is one of the reasons why any interpretation of the underlying physics of broadening is difficult.

Most of the work on x-ray diffraction line broadening was done on metals and alloys. Nowadays, it is widely accepted that plastic deformation in metals produces dislocation arrays, which divide crystallites into much smaller incoherently scattering domains. These dislocations produce a strain within the domains, causing strain broadening. In nonmetallic samples, the origins of broadening are somewhat different. Very often it is disregarded that, in the frame of current line-broadening theories, lattice strain is affected by other lattice imperfections, such as substitutions, vacancies, interstitials, site disorder, etc.. Although these effects in nonmetallic materials are often of a smaller importance than the size effect, only after a careful analysis is it possible to judge when some effects become "negligible". Therefore, it will be assumed throughout this chapter that both size and strain broadening are present simultaneously. Then, the physically broadened line profile is a convolution of size-broadened and strain-broadened line profiles.

3.1 Size broadening

Scherrer (1918) gave a basic definition of the "apparent" domain size:

$$\langle D \rangle_v = \frac{K\lambda}{\beta_S(2\theta) \cos\theta}; \quad \langle D \rangle_v = \frac{1}{\beta_S}. \tag{15}$$

The constant K depends on crystallite shape (Wilson 1962b), but generally is close to unity. Clearly, size broadening is independent of the reflection order, that is, independent of diffraction angle. This measure of domain size is a volume-weighted quantity.

Bertaut (1949) and Warren and Averbach (1950) independently derived another definition of domain size: the surface-weighted average. The Warren-Averbach method originally was developed for plastically deformed metals, but since its introduction it found successful applications to many other materials. The method is described extensively by Warren (1969). Each domain is represented by columns of cells along the a_3 direction normal to the diffracting planes (00l). All variables here are expressed as functions of column length $L = n|a_3|$, which is assumed to be positive, being a distance in real space between a pair of cells along direction of a_3. The size coefficient then reads as follows (Guinier 1963):

$$\begin{aligned} A_S(L) &= \int_L^\infty (1 - \frac{L}{L'}) \, p_v(L') \, \mathrm{d}L' \\ &= \frac{1}{\langle D \rangle_s} \int_L^\infty (L' - L) \, p_s(L') \, \mathrm{d}L', \end{aligned} \tag{16}$$

because it holds that

22

$$p_v(L) = \frac{L}{\langle D \rangle_s} p_s(L). \tag{17}$$

Here, the average surface-weighted domain size and the surface-weighted and volume-weighted column-length distribution functions are

$$\left(\frac{d \, A_S(L)}{d \, L} \right)_{L \to 0} = -\frac{1}{\langle D \rangle_s}; \tag{18}$$

$$p_s(L) \propto \frac{d^2 A_S(L)}{dL^2}; \quad p_v(L) \propto L \frac{d^2 A_S(L)}{dL^2}. \tag{19}$$

For a Voigt size-broadened profile, the size coefficient is given as a Fourier transform of (11):

$$A_S(L) = \exp(-2L\beta_{CS} - \pi L^2 \beta_{GS}^2). \tag{20}$$

By differentiating it twice, we obtain

$$\frac{d^2 A_S(L)}{dL^2} = [(2\pi L\beta_{GS}^2 + 2\beta_{CS})^2 - 2\pi \beta_{GS}^2] \, A_S(L). \tag{21}$$

Selivanov and Smislov (1991) showed that this may be a satisfactory approximation for some size-distribution functions.

If the column-length distribution functions are known, it is possible to evaluate mean values of respective distributions:

$$\langle D \rangle_{s,v} = \frac{\int\limits_0^\infty L p_{s,v}(L)\, dL}{\int\limits_0^\infty p_{s,v}(L)\, dL} . \tag{22}$$

Integrals of this type can be evaluated analytically (Prudnikov *et al.* 1986):

$$\int\limits_0^\infty z^m \exp(-bz^2 - cz)\, dz =$$
$$\frac{(-1)^m}{2} \left(\frac{\pi}{b} \right)^{1/2} \frac{\partial^m}{\partial c^m} \left[\exp\left(\frac{c^2}{4b} \right) \mathrm{erfc}\left(\frac{c}{2\sqrt{b}} \right) \right], \tag{23}$$

and for surface-weighted and volume-weighted domain size it follows that

23

$$\langle D \rangle_s = \frac{1}{2\beta_{CS}}; \quad \langle D \rangle_v = \frac{\exp(k_S^2)}{\beta_{GS}}\mathrm{erfc}(k_S) = \frac{1}{\beta_S}. \tag{24}$$

The same value of $\langle D \rangle_s$ is found from (18) and $\langle D \rangle_v$ is consistent with the Scherrer equation (15).

Two interesting points emerge here. From (21), it is clear that the second derivative of size coefficients, and consequently column-length distribution functions, can take negative values. Because any distribution function is, by definition, always positive, the Cauchy part in the size-broadened integral breadth must dominate. Inspection of (21) shows that for small L one must require

$$\beta_{CS} \geq (\pi/2)^{1/2}\beta_{GS}. \tag{25}$$

Otherwise, the "hook" effect will occur in a plot of size coefficients $A_S(L)$ versus L, that is, the plot will be concave downward for small L (Figure 5). The "hook" effect is a widely encountered problem in the Fourier analysis of line broadening, which results in overestimation of effective domain size. It is usually attributed to experimental errors connected with the truncation of the line profiles, and consequently the overestimation of background (Young *et al.* 1967). This is consistent with (25): if too high a background is estimated, it will cause the underestimation of the Cauchy content of the Voigt fitting function because the long tails will be truncated prematurely. This proves that the preset
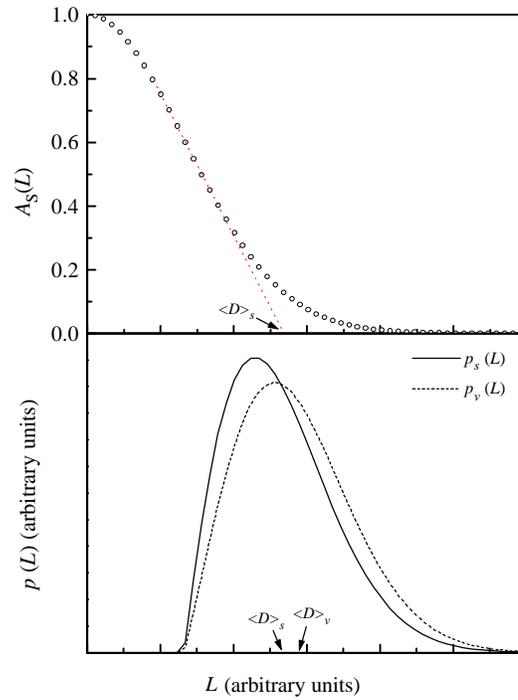

Fig. 5. The "hook" effect in the plot of size coefficients occurs because the Cauchy part of the fitting Voigt function is underestimated. This causes negative values (set to zero) of the column-length distribution functions for small L.

24

specimen-broadening function does not necessarily eliminate the "hook" effect. An important consequence of the "hook" effect is that domain sizes calculated from distribution functions (22) will not agree with values obtained from the integral breadths (24). Figure 5 shows that $<D>_s$ is obtained either as the intercept on the L axis of the straight portion of $A_S(L)$ or by the numerical integration of only the positive values of the surface-weighted column-length distribution function. However, so-obtained $<D>_s$ is erroneous as well as the value from (24), and the correct background should be found.

Also requiring close attention is the ratio of volume-weighted to surface-weighted domain size. Using (17) and (22) it follows that

$$<D>_v = \frac{<D^2>_s}{<D>_s}. \tag{26}$$

The Schwarz inequality requires that $<D^2>_s \geq <D>_s^2$, which determines that

$$<D>_v \geq <D>_s. \tag{27}$$

It is interesting to see the minimum value of this ratio for a Voigt size-broadened profile. From (24), using the physical solution of parabolic equation (14) for breadth of the Voigt function, it follows that

$$\frac{<D>_v}{<D>_s} = 2 \frac{\beta_{CS}}{\beta_S} = 4 \frac{\beta_{CS}}{\beta_{CS} + (\beta_{CS}^2 + 4 \beta_{GS}^2)^{1/2}}. \tag{28}$$

Strictly, the size-broadened profile can shift between Cauchy and Gauss extremes. After taking the inequality (25) into consideration, the ratio is bounded to the region

$$1.39 \leq \frac{<D>_v}{<D>_s} \leq 2. \tag{29}$$

The more accurate lower limit is obtained from (24):

$$\frac{<D>_v}{<D>_s} = 2\sqrt{\pi} k_S \exp(k_S^2) \operatorname{erfc}(k_S). \tag{30}$$

Generally, k_S can also change from zero to infinity. However, the minimum allowed value of k_S is determined by (25):

$$\frac{1}{\sqrt{2}} \leq k_S < \infty. \tag{31}$$

This implies that the ratio of domain sizes can change in a range

$$1.31 \approx (2\pi e)^{1/2} \operatorname{erfc}\left(\frac{1}{\sqrt{2}}\right) \leq \frac{<D>_v}{<D>_s} < 2. \tag{32}$$

Therefore, for a Voigt size-broadened profile, the ratio of volume-weighted to surface-weighted domain size cannot exceed 2. At this limit, $<D>_v = 2<D>_s$, and the size broadening is given only by

25

the Cauchy component. This is a case of pure Cauchy size broadening described earlier (Halder and Wagner 1966; Keijser *et al.* 1983). Alternatively, if the ratio is smaller than ~1.31, the Cauchy content of the Voigt size-broadened profile is underestimated. This indicates incorrect background and the "hook" effect. It may be noted that most experiments give the ratio $<D>_v/<D>_s$ in the specified range (see for instance the review by Klug and Alexander (1974)).

3.2 Strain broadening

Stokes and Wilson (1944) defined an "apparent" strain as

$$\eta = \beta_D(2\theta) \cot\theta. \tag{33}$$

The maximum (upper-limit) strain is derived as

$$e = \frac{\Delta d}{d} = \frac{\eta}{4} = \frac{\beta_D(2\theta)}{4 \tan\theta}; \quad e = \frac{\beta_D}{2 s}. \tag{34}$$

Langford *et al.* (1988) objected that the strain e has a doubtful meaning because it takes only the maximum value; there is no strain distribution that would be expected in a real material. Stokes and Wilson (1944) also defined a root-mean-square (RMS) value of strain e_{RMS} on the assumption of a Gauss strain distribution, which differs from e by a constant factor only: $e_{RMS} = (2/\pi)^{1/2}e$. From (34) it is clear that strain broadening is angle dependent, hence it will depend on the reflection order.

The RMS strain was not used extensively in the integral-breadth methods, but was adopted later in the Fourier Warren-Averbach approach. Note that these two RMS values of strain are equal only in the case of a Gaussian strain distribution, as explained below. If L is the undistorted distance, and distortion changes distance by ΔL, the component of strain in the a_3 direction (orthogonal to reflecting planes) averaged over cell-separation distance L can be defined as $\epsilon(L) = \Delta(L)/L$. It defines the distortion coefficients of the physically broadened line profile:

$$A_D(L,s) = <\exp(2\pi i s L \epsilon(L))>. \tag{35}$$

To obtain the strain component, it is necessary to approximate the exponential term. For not too large L the following approximation is useful:

$$< \exp(2\pi i s L \epsilon(L)) > \approx \exp(-2\pi^2 s^2 L^2 <\epsilon^2(L)>). \tag{36}$$

This relationship is exact if the strains $\epsilon(L)$ are distributed around the mean value according to the Gauss error function for all L values. In general it is valid up to the terms in $\epsilon^3(L)$ because it is expected that the strain distribution is symmetrical (Stokes and Wilson 1944).

Analogous to the size coefficient (20), the strain (distortion) coefficient of a Voigt strain-broadened profile (11) is

$$A_D(L) = \exp(-2L\beta_{CD} - \pi L^2 \beta_{GD}^2). \tag{37}$$

Comparison with (36) gives

$$<\epsilon^2(L)> \; = \; \frac{1}{s^2}\left(\frac{\beta_{GD}^2}{2\pi} + \frac{\beta_{CD}}{\pi^2}\frac{1}{L} \right).$$

(38)

Therefore, the mean-square strain decreases linearly with the averaging distance L. The expression for strain has both the L-dependent and L-independent contributions:

$$<\epsilon_V^2(L)> \; = \; <\epsilon_G^2> \; + \; <\epsilon_C^2(L)>$$

(39)

where

$$<\epsilon_G^2> \; = \; \beta_{GD}^2 / (2\pi s^2); \qquad <\epsilon_C^2(L)> \; = \; S_C / L;$$
$$S_C \; = \; \beta_{CD} / (\pi s)^2.$$

(40)

Wang *et al.* (1982) used (37) to model dislocation line broadening. Adler and Houska (1979) and Houska and Smith (1981) demonstrated that MSS can be represented by the sum of two terms, given by Cauchy and Gauss strain-broadened profiles. The Gauss constant-strain term may describe the uniform strain throughout domains caused by either fluctuation in the density of embedded atoms (Adler and Houska 1979) or by dislocation-cell walls (Kamiyama *et al* 1990). The Cauchy part is determined by strains around individual dislocations (Rothman and Cohen 1971). The Cauchy parameter S_C defines the skewness of the $<\epsilon_V^2(L)>$ curve for small L. For larger distances L, mean-square strain saturates at the pure-Gauss value $<\epsilon_G^2>$. In the case of the pure-Gauss strain broadening ($\beta_{DC}=0$), the MSS is independent of L (see also Halder and Wagner (1966) and Keijser *et al.* (1983)):

$$<\epsilon^2>^{1/2} \; = \; \left(\frac{2}{\pi} \right)^{1/2} e.$$

(41)

There is no obvious connection between RMSS and e if the strain-broadened line profile contains a Cauchy component. However, in the case of the pure-Cauchy strain-broadened line profile, with (34), which is assumed regardless of the particular line-profile function, and (38), it follows that the two measures of strain are related:

$$e \; = \; (\pi^2 / 2)\, L\, s <\epsilon_C^2(L)>.$$

(42)

In the general case, the maximum strain e is determined from the integral breadth of a Voigt function:

$$2\,e\,s \; = \; \beta_{GD}\exp(-k_D^2) / \operatorname{erfc}(k_D).$$

(43)

In combination with (38), it follows that

$$\frac{e}{\langle\epsilon_V^2(L)\rangle^{1/2}} = \left(\frac{\pi}{2}\right)^{1/2} \frac{\exp(-k_D^2)}{\mathrm{erfc}(k_D)} \frac{1}{\left(1 + \dfrac{2k_D^2}{\beta_{CD}L}\right)^{1/2}}.$$

(44)

This function is plotted in Figure 6 for different values of the product $\beta_{CD}L$. In the Gauss limit ($k_D \to 0$), the ratio is constant, $(\pi/2)^{1/2}$, as pointed out above. It is interesting to consider the ratio when the Cauchy part dominates. Clearly, the ratio of strains can be either larger or smaller than unity, which depends on values of both β_{CD} and L. Let us make a reasonable estimate for the most common values for the Cauchy extreme. For large k_D, the asymptotic expansion of the complementary error function may be used (Abramowitz and Stegun 1964):

$$\pi^{1/2} z \exp(z^2)\, \mathrm{erfc}(z) \sim$$
$$1 + \sum_{m=1}^{\infty} (-)^m (1\cdot3\cdot5\cdots(2m-1))/(2z^2)^m.$$

(45)

We write (45) with k_D as

$$\mathrm{erfc}(k_D) = (\exp(-k_D^2)/\pi) \sum_{m'=0}^{m-1} (-)^{m'} \Gamma(m'+1/2)/k_D^{(2m'+1)}$$
$$+ R_m(k_D^{-(2m+1)}).$$

(46)

Here, Γ denotes the gamma function. For large and real argument, in the first approximation (with
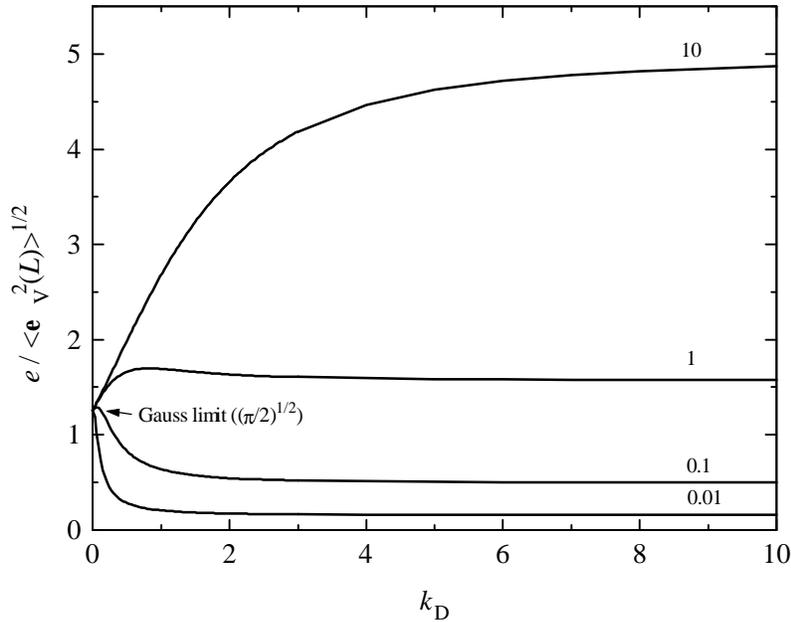

Fig. 6. Ratio of maximum strain, e, to the RMSS, $\langle\epsilon_V^2(L)\rangle^{1/2}$, as a function of the Voigt parameter, $k_D = \beta_{CD}/(\pi^{1/2}\beta_{GD})$, for different values of the product $\beta_{CD}L$.

$m' = 0$ and neglecting the remainder in (46)), (44) with $2k_D^2/(\beta_{CD}L) \gg 1$ gives

$$e\,/\,<\epsilon_V^2(L)>^{1/2} \approx (\pi/2)(\beta_{CD}L)^{1/2}, \tag{47}$$

which leads to (42) for the Cauchy limit ($\beta_{CD} = 2es$):

$$e\,/\,<\epsilon_C^2(L)>^{1/2} = (\pi/2)(2\,e\,s\,L)^{1/2}. \tag{48}$$

Because the product Ls is larger than unity even for small L (it was customary to compare RMSS at the arbitrary value of $L = 50$ Å), the ratio $e\,/\,<\epsilon_V^2(L)>^{1/2}$ will depend on the strain magnitude. Usually, strain falls in the range 10^{-2}-10^{-3} and it is averaged over a distance comparable to the coherent domain size. For example, $<D_V>_{v,s}\,s = <D_V>_{v,s}/d = N$, the average number of reflecting planes perpendicular to the diffracting vector, is always a large number, and the product Ne is roughly constant and close to unity. A rough estimate from (48) gives a factor of 2 for the strains ratio. Therefore, it may be concluded that the upper limit of strain e should not differ much from the RMSS in the whole range between the Gauss and Cauchy extremes of the strain-broadened Voigt profile:

$$e\,/\,<\epsilon_V^2>^{1/2} = (\pi/2)^{1/2} \approx 1.253 \qquad \text{Gauss strain broadening;} \tag{49}$$

$$0.5 \lesssim e\,/\,<\epsilon_V^2(L)>^{1/2} \lesssim 2 \qquad\qquad \text{otherwise.} \tag{50}$$

3.3 Separation of size and strain broadening

From the preceding paragraphs, it is evident that size broadening is angle independent, whereas strain broadening depends on diffracting angle. This is a basis for their separation. Unfortunately, it is immediately obvious from the form of Stokes and Wilson (1944) [(34)] and Warren (1969) [(35)] definitions of the strain that results will generally disagree. Nowadays, two routes are used mostly: Warren-Averbach method (Warren and Averbach 1952) and the integral-breadth methods. Because they use differently defined parameters, the results disagree. However, it will be shown that this limitation can be overcome. Among the integral-breadth methods, single-line approaches and the so-called simplified multiple-line methods will not be treated here. A review was given by Klug and Alexander (1974). A survey of single-line methods was authored by Delhez *et al.* (1982). Balzar and Popović (1996) recently published a comparative study of simplified integral-breadth methods.

3.3.1 Warren-Averbach method

Because convolutions of size-broadened and strain-broadened profiles in real space are calculated simply as products of their respective Fourier transforms, the Fourier coefficients of a

physically broadened line profile are the product of size and distortion coefficients:

$$A(L,s) = A_S(L) A_D(L,s) \qquad (51)$$

where coefficients are given by (16) and (35)

$$A_S(L) = \frac{1}{<D>_s} \int_L^\infty (L' - L) \, p_s(L') \, \mathrm{d}L';$$
$$A_D(L,s) = <\exp(2\pi i s L \epsilon(L))>. \qquad (52)$$

By taking the approximation (36) for the distortion coefficient, the well-known Warren-Averbach method of separation of size and strain broadening is obtained:

$$\ln A(L,s) = \ln A_S(L) - 2\pi^2 s^2 L^2 <\epsilon^2(L)>. \qquad (53)$$

They derived this relationship in a different way, by expanding the logarithm of the cosine in a power series. It must be noted that, regardless of its derivation, the Warren-Averbach method does not necessarily assume a Gauss strain distribution, or that mean-square strain is independent of distance L. However, the Warren-Averbach approach becomes exact in the case of Gaussian distribution of $\epsilon(L)$ for each L.

3.3.2 Voigt multiple-line integral-breadth methods

In preceding paragraphs, consequences of both size-broadened and strain-broadened Voigt profile were discussed. A convolution of two Voigt functions, being a physically broadened profile, is also a Voigt function. The size and strain (distortion) integral breadths of Cauchy and Gauss parts are combined simply:

$$\beta_C = \beta_{CS} + \beta_{CD}(s); \qquad (54)$$

$$\beta_G{}^2 = \beta_{GS}{}^2 + \beta_{GD}{}^2(s). \qquad (55)$$

These relations assume that the size component does not depend on s, whereas the strain component does depend on s. The actual s dependence is determined by the strain model chosen. Currently, there are two possible models:

(i) Stokes and Wilson (1944) definition of "apparent" strain requires that both β_{CD} and β_{GD} be linear functions of s. This approach is built into all simplified integral-breadth methods and introduced in the multiple-line Voigt method by Langford (1980):

$$\beta_C = \beta_{CS} + \beta_{CD} \frac{s}{s_0}; \qquad (57)$$

$$\beta_G{}^2 = \beta_{GS}{}^2 + \beta_{GD}{}^2 \frac{s^2}{s_0{}^2}. \qquad (56)$$

Here, β_{CD}/s_0 and $\beta_{GD}{}^2/s_0{}^2$ are constant for the pattern and taken conveniently for the first peak.

(ii) Warren (1969) definition of mean-square strain requires that the Cauchy and Gauss distortion integral breadths depend differently on s (Balzar and Ledbetter 1993) and the same relations read

$$\beta_C = \beta_{CS} + \beta_{CD} \frac{s^2}{s_0^2}; \tag{58}$$

$$\beta_G{}^2 = \beta_{GS}{}^2 + \beta_{GD}{}^2 \frac{s^2}{s_0^2}. \tag{59}$$

Here, $\beta_{CD}/s_0{}^2$ and $\beta_{GD}{}^2/s_0{}^2$ are constant for the pattern and "apparent" strain is not independent of diffraction angle because β_{CD} and β_{GD} dependent differently on s. The unknowns β_{CS}, β_{CD}, β_{GS}, and β_{GD} are obtained by plotting both β_C and $\beta_G{}^2$ as functions of s^2 for multiple orders of reflections. This method will be designated as the "double-Voigt" method for brevity, although Langford's (1980) multiple-line Voigt method used the same assumption for size-broadened and strain-broadened integral breadths, that is the Voigt functions.

Both multiple-line Voigt methods will give the simplified integral-breadth methods as limiting cases. However, the results will be different in general because a different definition of strain is adopted.

31

3.3.3 Size-strain analysis of W and MgO

If (58) and (59) are combined with (38) at $s = s_0$, which is taken constant for the pattern, one obtains

$$-(2L\beta_C + \pi L^2\beta_G^2) = -(2L\beta_{CS} + \pi L^2\beta_{GS}^2)$$
$$- 2\pi^2 s^2 L^2 <\epsilon^2(L)>. \tag{60}$$

The first two terms are logarithms of $A(L,s)$ and $A_S(L)$ respectively and the equivalence of the "double-Voigt" with the Warren-Averbach method (53) for identical Fourier coefficients $A(L,s)$ becomes evident (Balzar and Ledbetter 1993). Therefore, instead of tedious graphical analysis of Fourier coefficients, one can directly calculate both surface-weighted and volume-weighted domain size from (24), mean-square strain for each L from (38), and both surface-weighted and volume-weighted column-length distribution functions from (19) and (21). Although the results of Stokes deconvolution and convolution fitting gave similar physically broadened profiles of both the W and MgO specimens, in practice, the differences will appear in the subsequent analyses. Thus, we applied the Warren-Averbach method to the Stokes Fourier-deconvoluted coefficients and "double-Voigt" method to the refined parameters of preset physically broadened Voigt profile to see which parameters show largest disagreement. Table 5 gives a comparison of results for the two methods.

Figure 7 gives a plot of $\ln A(L)$ as a function of s^2 for W. It agrees well with results given by McKeehan and Warren (1953). The size coefficients, obtained from real Fourier coefficients, are plotted in Figure 8 as a function of distance L. Interestingly, they are almost linear, which indicates a Laue size-broadened line profile. This is expected for small crystals, but often approximated with a Cauchy function (see, for instance, Warren (1959)). It is seen from Table 5 that the size-broadened profile calculated by the "double-Voigt" method is approximately a pure Cauchy function (β_{GS}^2 has a small negative value), and the full curve in Figure 8 is an exponential. This is a known case of pure-Cauchy size broadening, which implies $<D>_v = 2<D>_s$. Domain size determined from the initial slope of $A_S(L)$ is in error because of a small "hook" effect. When corrected, initial Fourier coefficients agree well with the curve obtained from the Voigt function. It is not likely that this "hook" effect originates from the background overestimation, because it would also show through the "double-Voigt" method because background was identical for both cases. Therefore, it may be caused by the uncertainty in a first few Fourier coefficients.

Figure 9 shows MSS as a function of distance L. Inherent to the "double-Voigt" analysis, it falls off with $1/L$, whereas MSS calculated by the Warren-Averbach method does not follow it for intermediate and large L, which may be caused by uncertainty of Fourier coefficients.

Table 5. Comparison of results obtained by application of Warren-Averbach (W-A) and the "double-Voigt" (V-V) methods. All symbols defined in text. Standard uncertainties (s.u.) reflect the random measurement and different fitting errors. They were calculated using the computer program BREADTH (Balzar 1995) according to errors given by Balzar (1993), but for multiple reflections.

		W	MgO
β_S		2.23	7.84
β_{CS}		2.23	6.47
β_{GS}	$(10^{-3}\,\text{Å}^{-1})$	imaginary	2.73
β_D		1.66	2.44
β_{CD}		0.334	negative
β_{GD}		1.44	2.44
$<D>_s$ (W-A)		340,209[*]	79
$<D>_s$ (V-V)	(Å)	224(12)	77(1)
$<D>_v$ (V-V)		448(24)	128(1)
$<\epsilon^2(a_3)>^{1/2}$ (W-A)		5.10	2.14[**]
$<\epsilon^2(a_3)>^{1/2}$ (V-V)	(10^{-3})	4.79(18)	1.45(2)
$<\epsilon^2(<D>_s/2)>^{1/2}$ (W-A)		1.53	2.14[**]
$<\epsilon^2(<D>_s/2)>^{1/2}$ (V-V)		1.78(6)	1.45(2)
$<\epsilon^2(<D>_s/2)>^{1/2}$ (V-V)		1.55(6)	1.45(2)

[*] After the "hook"-effect correction.
[**] Assumes that strains are approximately independent of *L*.

It is worthwhile to note that $\beta_S > \beta_D$. That is, against expectation, strain does not appear to be a major source of broadening for ball-milled W.

The studies of cold-worked W gave very similar results for both domain size and strain, regardless of the deformation procedure: McKeehan and Warren (1953) gave values for thoriated-tungsten filings $<D>_s = 200$ Å, $<\epsilon^2(<D>_s / 2)>^{1/2} \approx 2.2 \cdot 10^{-3}$; Aqua and Wagner (1964) reported for tungsten filings $<D>_s = 220$ Å, $<\epsilon^2(<D>_s / 2)>^{1/2} \approx 2.7 \cdot 10^{-3}$; Berkum (1994) for ball-milled tungsten $<D>_s = 170$ Å, $<\epsilon^2(<D>_s / 2)>^{1/2} = 1.3 \cdot 10^{-3}$. Evidently, regardless of type of deformation, there is
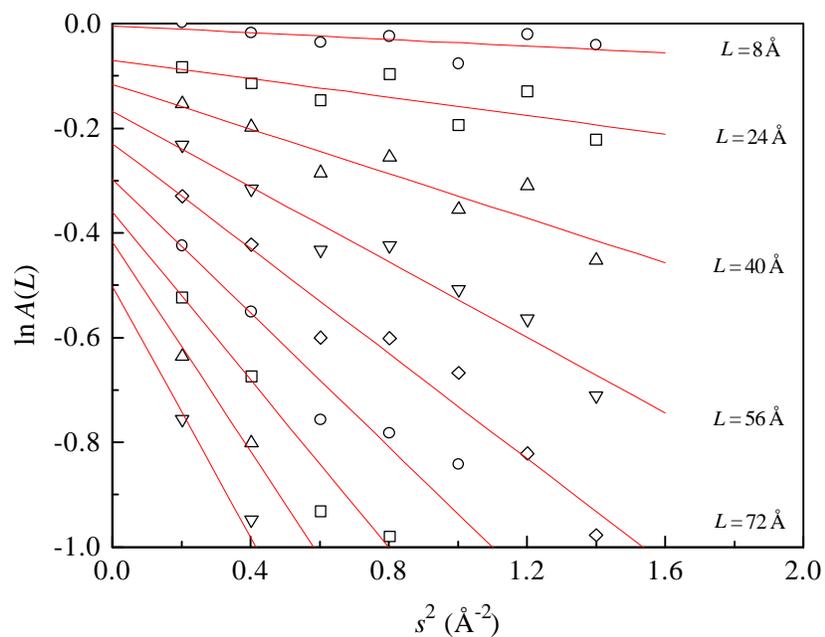
Fig. 7. Plot of the first nine odd real Fourier coefficients for seven reflections of W. The ordinate intercepts yield size coefficients and slopes the mean-square strains.
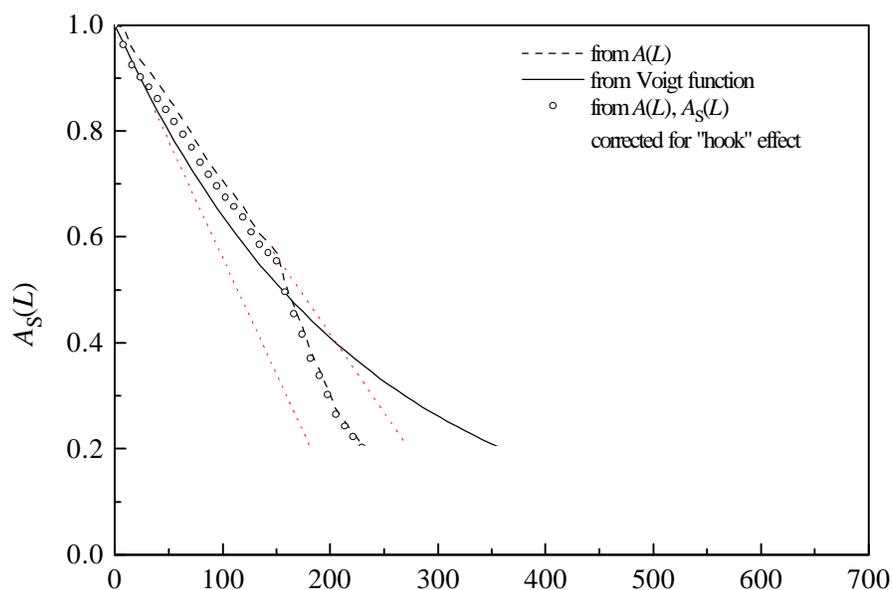

Fig. 8. Size coefficients determine the surface-weighted domain size for W which estimates to ~ 224 Å from the "double-Voigt" method and ~ 340 Å from the Warren-Averbach analysis of $A(L)$. After the "hook"-effect correction, the value is closer to that obtained by "double-Voigt" method.
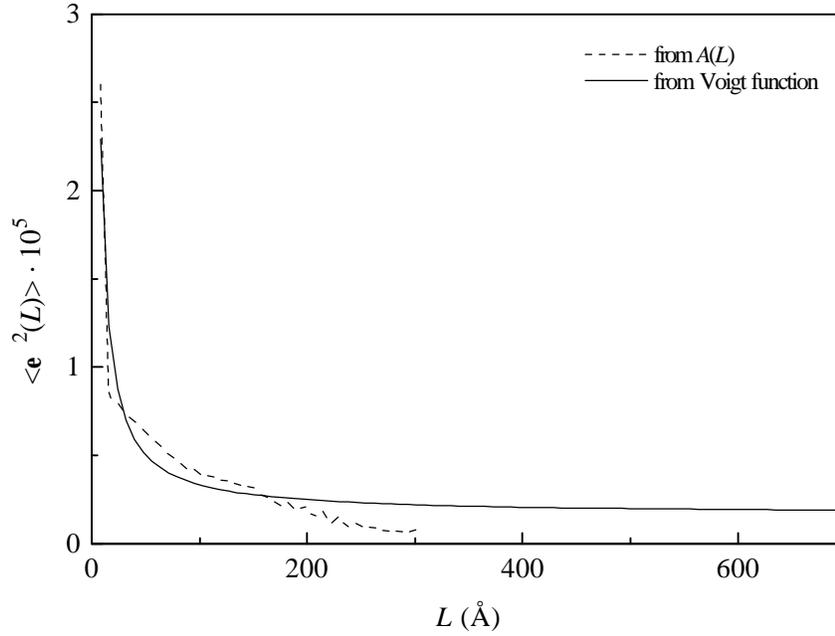
Fig. 9. Mean-square strain as a function of averaging distance for the W specimen.

a maximum density and energetically favorable arrangement of dislocations. Only Wagner *et al.* (1992) reported as small as $<D>_s = 35$ Å and strain up to $<\epsilon^2(<D>_s / 2)>^{1/2} \approx 6\cdot10^{-3}$. This kind of deformation was produced after 20 h in a high-energy ball mill and explained by the incorporation of Fe and Cr impurities into W particles.

The results for MgO provide equal interest. From the Williamson-Hall plot (Williamson and Hall 1953) (Figure 10) it is seen that three reflections can be analyzed simultaneously. Also, the relatively small slope indicates a small strain. Moreover, it is observed that $\beta_C(s)$ has slightly negative slope, meaning that the strain-broadened profile is a Gauss function. More accurate results are found in Table 5; β_{CD} has a small negative value. In case of pure-Gauss strain broadening, MSS is independent of L and relates to the "maximum" strain e from the integral-breadth methods, according to (49). Figure 11 shows that Warren-Averbach analysis gives somewhat larger strain. Although values scatter, it is reasonable to assume that it is constant for 30 Å $< L <$ 120 Å.
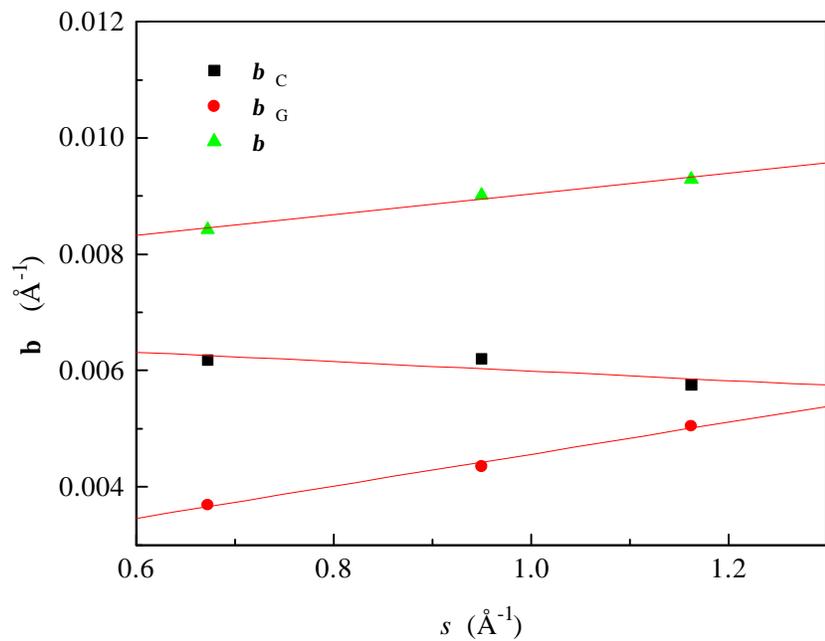
Fig. 10. Williamson-Hall plot (Cauchy-Cauchy approximation) for 220, 400, and 422 reflections of MgO.
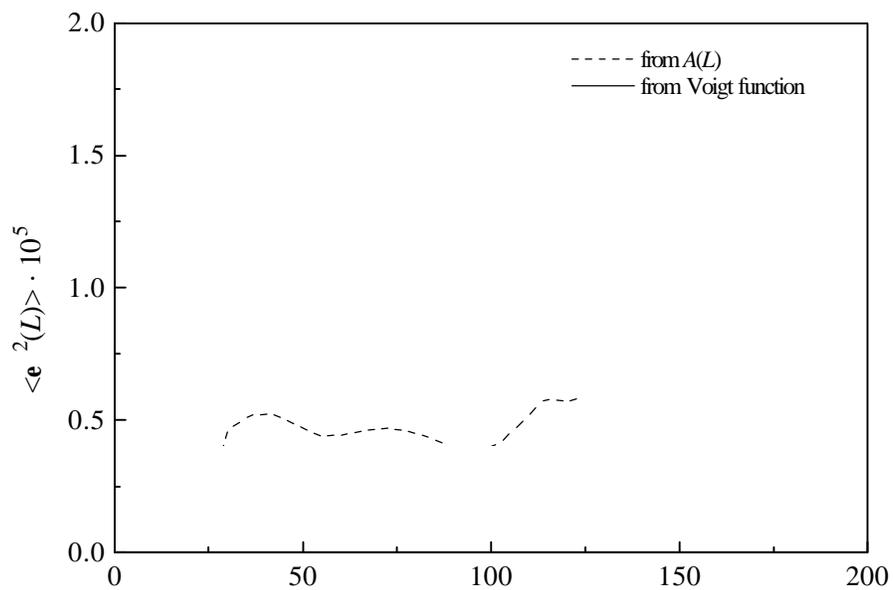

Fig. 11. Mean-square strain as a function of averaging distance for the MgO specimen.
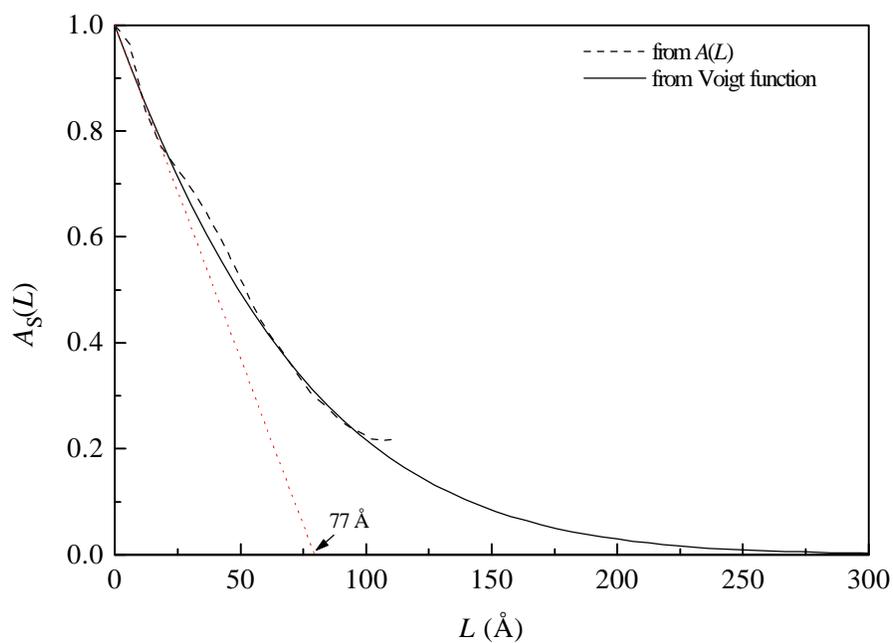
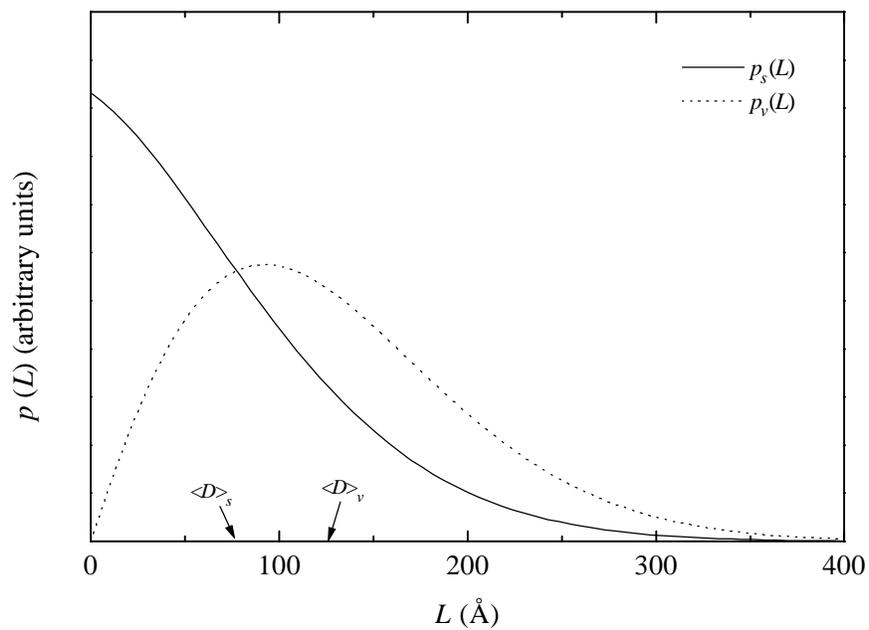**Fig. 12.** Size coefficients for the MgO specimen.

Fig. 13. Surface-weighted column-length distribution function, $p_s(L)$, and volume-weighted column-length distribution function, $p_v(L)$, for the MgO specimen.

For the first three harmonic numbers, MSS is not real, which is, strictly speaking, also true for the "double-Voigt" method, because β_{CD} is negative. Although small, this part dominates for smallest L values, according to (38). Negative values of MSS for smallest L values may result from small measurement errors, because at this region, MSS change rapidly and are very sensitive to the even small uncertainties in Fourier coefficients. From Figure 12 and Table 5, almost identical results for $<D>_s$ follow from the Warren-Averbach and "double-Voigt" methods. It is often assumed that a Cauchy function can model the size-broadened profile satisfactorily unlike the strain-broadened profile which some authors model with a Voigt function. Analysis here shows that the (dominant) size broadening in MgO shows a significant Gauss content, which was noted previously (Young and Desai 1989). Therefore, a Voigt function as the size-broadened profile seems a better choice.

In principle, it is possible to obtain the column-length distribution function by taking a second derivative of the size coefficients. However, it is clear that there are at least two obstacles: (i) if strain distribution is not exactly Gaussian for every L, size coefficients are accurate enough only for small harmonic numbers and/or negligible strain; (ii) even if the Gaussian strain distribution can be proven, the high-order size coefficients are unreliable, preventing computation of the column-length distribution function. Few techniques were used to deal with this problem: successive convolution unfolding method (Ergun 1968), smoothing, and iterative methods (Păuseşcu *et al.* 1974; Le Bail and Louër 1978). The "double-Voigt" method gives a smooth distribution function, as shown in Figure 13. How reliable they are for large L will again depend on the nature of the strain distribution. If they agree with the Warren-Averbach method for small L, they certainly give more reliable information about the true column-length distribution function than the Warren-Averbach method. In the case of MgO, strain is small. By taking $s = 1.16$ Å^{-1} for the 422 MgO line and $<\epsilon^2>^{1/2} = 1.45 \cdot 10^{-3}$ from Table 5, the term $2\pi^2 s^2 L^2 <\epsilon^2>$ becomes equal to unity for $L = 133.8$ Å, that is, about the value of $<D>_v$.

These two examples show that, against expectations, it is difficult to treat any case as either

size-only or strain-only broadening. MgO does show a prevailing size effect, but the value of strain, as obtained from the Warren-Averbach analysis at $<D>_s$ / 2, is larger than for W! Also, the size-broadened profile, being a dominant part of the physically broadened profile, has a significant Gauss content. The W example shows again that it is unlikely to find a sample with the strain-only broadening. Preparing a specimen without small particles through fractional sedimentation or any other means does not yield the desired effect, because diffraction incoherency exists on the subgrain level.

4 Concluding remarks

Nowadays, diffraction is done using much different tools than decades ago both regarding instrumentation and especially data analysis. Numerous computer programs give solutions for almost any task, and the amount of information obtainable from a simple powder-diffraction scan is astonishing. Hence, it is likely that line-broadening analysis will become a part of routine program output, together with line positions, intensities, lattice parameters, *etc*. Full-pattern-analysis software, such as some Rietveld refinement programs, already includes refinable parameters corresponding to domain size and strain. Unfortunately, inspection of line broadening is rarely a standard procedure. Being so automated, line-broadening analysis is very often inaccurate because of inadequate models used in most Rietveld programs. Instead, the approach based on a Voigt function (Balzar and Ledbetter 1995), which is generally applicable and probably much more accurate than current models, may be more useful.

A frequent objection is that any phenomenological approach with a single analytical function may not correspond to the more realistic model based on physical causes of broadening for a particular specimen. It would be very inconvenient and complicated at this moment to build such a specific approach in a widely applicable Rietveld-refinement program. This is why line shapes in Rietveld programs in the past were not modeled in terms of physically sound parameters. As they are

introduced more and more in the codes, it is wise to find a balance between the accuracy of parameters refined and reasonable universality of a model. Another common objection to the presumed analytical functions in line-broadening analysis is that data are being "pushed" into the model. Although it is possible to lose useful information by adopting a preset model, this approach should always be weighted against the actually useless information if results are hampered by the inherent errors of some model-independent method.

During decades of research, it became more and more obvious that neither Cauchy nor Gauss functions can adequately model diffraction line broadening. Here it was shown that a model based on a Voigt function may be more realistic and accurate. Moreover, previously considered as divergent approaches, namely the Warren-Averbach analysis and the integral-breadth methods, are consistently related. Some common occurrences in Warren-Averbach analysis, particularly the "hook" effect, functional dependence of mean-square strain on averaging distance, and ratio of volume-weighted to the surface-weighted domain size, all follow from the "double-Voigt" model. Some possible limitations of Voigt-based models are both of conceptual (asymmetric physically broadened profiles) and practical (observed line profiles may fall below the Voigt-Cauchian limit) nature. We may have some better function of choice in the future, but the Voigt function may still prove to be a satisfactory approximation in most cases.

Acknowledgments

References

Abramowitz, M. and Stegun, I. A., editors. (1964). *Handbook of Mathematical Functions*, p. 298. Washington, D.C.: National Bureau of Standards.

Adler, T. and Houska, C. R. (1979). *J. Appl. Phys.* **50**, 3282-3287.

Ahtee, M., Unonius, L., Nurmela, M. and Suortti, P. (1984). *J. Appl. Cryst.* **17**, 352-357.

Aqua, E. N. and Wagner, C. N. J. (1964). *Phil. Mag.* **9**, 565-589.

Balzar, D. (1992). *J. Appl. Cryst.* **25**, 559-570.

Balzar, D. (1993). *J. Res. Natl. Inst. Stand. Technol.* **98**, 321-353.

Balzar, D. (1995). *J. Appl. Cryst.* **28**, 244-245.

Balzar. D. and Ledbetter, H. (1993). *J. Appl. Cryst.* **26**, 97-103.

Balzar, D. and Ledbetter, H. (1995). *Adv. X-ray Anal.* **38**, 397-404.

Balzar, D. and Popović, S. (1996). *J. Appl. Cryst.* **29**, 16-23.

Balzar, D., Stephens, P. W. and Ledbetter, H. (1997a). *Adv. X-ray Anal.* **40**, in press.

Balzar, D., Stephens, P. W. and Ledbetter, H. (1997b), in preparation.

Berkum, J. G. M. van, Sprong, G. J. M., Keijser, Th. H. de, Delhez, R. and Sonneveld, E. J. (1995). *Powder Diffr.* **10**, 129-139.

Berkum, J. G. M. van (1994*). Ph.D. Thesis*, p. 173. Delft, The Netherlands: Delft University of Technology.

Bertaut, E. F. C. (1949). *R. Acad. Sci.* **228**, 492-494.

Caglioti, G., Paoletti, A. and Ricci, F. P. (1958). *Nucl. Instrum.* **3**, 223-228.

Delhez, R., Keijser, Th. H. de and Mittemeijer, E. J. (1980). In *Accuracy in Powder Diffraction*, NBS Special Publication No. 567, edited by S. Block and C. R. Hubbard, pp. 213-253. Washington, D.C.: National Bureau of Standards.

Delhez, R., Keijser, Th. H. de and Mittemeijer, E. J. (1982). *Fresenius Z. Anal. Chem.* **312**, 1-16.

Delhez, R., Keijser, Th. H. de, Mittemeijer, E. J. and Langford, J. I. (1986). *J. Appl. Cryst.* **19**, 459-466.

Delhez, R., Keijser, Th. H. de, Mittemeijer, E. J. and Langford, J. I. (1988). *Aust. J. Phys.* **41**, 213-227.

Enzo, S., Fagherazzi, G., Benedetti, A. and Polizzi, S. (1988). *J. Appl. Cryst.* **21**, 536-542.

Ergun, S. (1968). *J. Appl. Cryst.* **1**, 19-23.

Groma, I., Ungár, T. and Wilkens, M. (1988). *J. Appl. Cryst.* **21**, 47-53.

Guinier, A. (1963). *X-ray Diffraction*, San Francisco: W. H. Freeman.

Halder, N. C. and Wagner, C. N. J. (1966). *Acta Cryst.* **20**, 312-313.

Hall, M. M. Jr, Veeraraghavan, V. G., Rubin, H. and Winchell, P. G. (1977). *J. Appl. Cryst.* **10**, 66-68.

Houska, C. R. and Smith, T. M. (1981). *J. Appl. Phys.* **52**, 748-754.

Howard, S. A. and Snyder, R. L. (1989). *J. Appl. Cryst.* **22**, 238-243.

Howard, S. A. and Preston, K. D. (1989). In *Modern Powder Diffraction*, Vol. **20**, edited by D. L. Bish and J. E. Post, pp. 217-275. Washington, D.C.: The Mineralogical Society of America.

Kalceff, W., Armstrong, N. and Cline, J. P. (1995). *Adv. X-ray Anal.* **38**, 387-395.

Kamiyama, T., Shinohara, T., Tomiyoshi, S., Minonishi, Y., Yamamoto, H., Asano, H. and Watanabe, N. (1990). *J. Appl. Phys.* **68**, 4741-4750.

Keijser, Th. H. de, Mittemeijer, E. J. and Rozendaal, H. C. F. (1983). *J. Appl. Cryst.* **16**, 309-316.

Klug, H. P. and Alexander, L. E. (1974). *X-ray Diffraction Procedures*, 2nd edition, pp. 618-708. New York: John Wiley and Sons.

Krivoglaz, M. A. and Ryaboshapka, K. P. (1963). *Phys. Met. Metall.* **15**, 14-26.

Kuhn, H.-A., Biermann, H., Ungár, T. and Mughrabi, H. (1991). *Acta Metall. Mater.* **39**, 2783-2794.

Langford, J. I. (1978). *J. Appl. Cryst.* **11**, 10-14.

Langford, J. I. (1980). In *Accuracy in Powder Diffraction*, NBS Special Publication No. 567, edited by S. Block and C. R. Hubbard, pp. 255-269. Washington, D.C.: National Bureau of Standards.

Langford, J. I., Delhez, R., Keijser, Th. H. de and Mittemeijer, E. J. (1988). *Aust. J. Phys.* **41**, 173-187.

Le Bail, A. and Louër, D. (1978). *J. Appl. Cryst.* **11**, 50-55.

McKeehan, M. and Warren, B. E. (1953). *J. Appl. Phys.* **24**, 52-56.

Păuseşcu, P., Mănăilă, R., Popescu, M. and Jijovici, E. (1974). *J. Appl. Cryst.* **7**, 281-286.

Pawley, G. S. (1981). *J. Appl. Cryst.* **14**, 357-361.

Prudnikov, A. P., Brychkov, Yu. A. and Marichev, O. I. (1986). *Integrals and Series*, Vol. **1**, p. 344.

Amsterdam, The Netherlands: Gordon and Breach.

Reynolds, R. C. (1989). In *Modern Powder Diffraction*, Vol. **20**, edited by D. L. Bish and J. E. Post, pp. 145-182. Washington, D.C.: The Mineralogical Society of America.

Rietveld, H. M. (1967). *Acta Cryst.* **22**, 151-152.

Rothman, R. L. and Cohen, J. B. (1971). *J. Appl. Phys.* **42**, 971-979.

Scherrer, P. (1918). *Nachr. Gött.* **2**, 98-100.

Schoening, F. R. L. (1965). *Acta Cryst.* **18**, 975-976.

Schwartz, L. H. and Cohen, J. B. (1977). *Diffraction from Materials*, p. 391. New York: Academic Press.

Selivanov, V. N. and Smislov, E. F. (1991). *Zavod. Lab.* **57**, 28-29.

Skilling, J. and Bryan, R. K. (1984). *Mon. Not. R. Astr. Soc.* **211**, 111-124.

Stokes, A. R. (1948). *Proc. Phys. Soc. London* **61**, 382-391.

Stokes, A. R. and Wilson, A. J. C. (1944). *Proc. Phys. Soc. London* **56**, 174-181.

Suortti, P., Ahtee, M. and Unonius, L. (1979). *J. Appl. Cryst.* **12**, 365-369.

Taupin, D. (1973). *J. Appl. Cryst.* **6**, 266-273.

Toraya, H. (1986). *J. Appl. Cryst.* **19**, 440-447.

Twomey, S. (1963). *J. Assoc. Comput. Mach.* **10**, 97-101.

Wagner, C. N. J., Yang, E. and Boldrick, M. S. (1992). *Adv. X-ray Anal.* **35**, 585-592.

Wang, Y., Lee, S. and Lee, Y. (1982). *J. Appl. Cryst.* **15**, 35-38.

Warren, B. E. (1959). In *Progress in Metal Physics*, Vol. **8**, pp. 147-202. London: Pergamon Press.

Warren, B. E. (1969). *X-ray Diffraction*, pp. 251-314. New York: Addison-Wesley.

Warren, B. E. and Averbach, B. L. (1950). *J. Appl. Phys.* **21**, 595-599.

Warren, B. E. and Averbach, B. L. (1952). *J. Appl. Phys.* **23**, 497.

Wertheim, G. K., Butler, M. A., West, K. W. and Buchanan, D. N. E. (1974). *Rev. Sci. Instrum.* **11**, 1369-1371.

Wilkens, M. (1984). In *Microstructural Characterization of Materials by Non-Microscopical Techniques,* edited by N. H. Andersen, M. Eldrup, N. Hansen, D. J. Jensen, T. Leffers, H. Lilholt, O. B. Pedersen and B. N. Singh, pp. 153-168. Roskilde, Denmark: Risø National Laboratory.

Williamson, G. K. and Hall, W. H. (1953). *Acta Met.* **1**, 22-31.

Wilson, A. J. C. (1962a) *Nature (London)* **193**, 568-569.

Wilson, A. J. C. (1962b). *X-ray Optics*, 2nd edition, London: Methuen.

Young, R. A. and Desai, P. (1989). *Arch. Nauk Mater.* **10**, 71-90.

Young, R. A., Gerdes, R. J. and Wilson, A. J. C. (1967). *Acta Cryst.* **22**, 155-162.

Young, R. A. and Wiles, D. B. (1982). *J. Appl. Cryst.* **15**, 430-438.